

Long Range Sound Propagation in a Turbulent Atmosphere Within the Parabolic Approximation

Ph. Blanc-Benon, L. Dallois, D. Juvé

Ecole Centrale de Lyon, Centre Acoustique, LMFA, UMR CNRS 5509, BP 163, 69131 Ecully Cedex, France

Summary

The characteristics of acoustic waves propagating in the atmosphere are mainly determined by the environment. Acoustic signals vary both in space and time, and the dominant source of this variability is the turbulence of the atmospheric boundary layer. The influence of temperature and velocity random fluctuations have been demonstrated in many experimental studies. During the last decade significant progress have been made in the modelling of sound propagation over distances ranging from hundreds meters to kilometers, and the agreement between calculated and measured fields have been greatly improved. New developments appear in two domains: the numerical simulation of random fields and the parabolic-equation method. We will evaluate these new wide-angle parabolic equations through a series of numerical experiments. Different types of velocity fields will be used in these evaluations: a profile of sound speed combined with a velocity distribution, and a velocity field having random spatial fluctuations over a range of spatial scales. The objective is to determine the effect of using a more accurate PE in modelling acoustic propagation in inhomogeneous moving media.

PACS no. 43.20.Bi, 43.20.Fn, 43.20

1. Introduction

Sound waves propagate through a material medium and are influenced by two principal characteristics: the sound speed (celerity) of the medium, and the velocity of the medium. Variations in sound speed across the medium, for example, can create focusing and defocusing and affect the entire sound field. If the medium is not stationary, i.e., it exhibits mean motion or velocity fluctuations, sound waves are convected by the mean motion of the field and scattered by velocity gradients. For numerical simulations of outdoor sound propagation, parabolic equations have been derived using the approximation of the effective sound speed. In this conventional approach the real moving atmosphere is replaced by a hypothetical motionless medium with the effective sound speed $c_{eff} = c + v_x$, where v_x is the wind velocity component along the direction of propagation between source and receiver. When the source and receiver are close to the ground, the preferred direction of sound propagation is nearly horizontal, and standard parabolic equations can be used to predict sound pressure levels. However, in many problems of atmospheric acoustics, refracted sound waves and those scattered by turbulence propagate in directions which may significantly differ from the horizontal axis. Recently Ostashev *et al.* [1], Dallois *et al.* [2], Dallois [3] derived new wide-angle parabolic equations which do maintain the vector properties of the velocity of the medium.

2. Parabolic equations for moving media

A rigorous way to incorporate the effects of a velocity field is to begin with the fundamental equations of fluid mechanics

and derive a wave equation which includes the velocity. In the limits of linear acoustic theory, such a wave equation can be derived as the sum of a d'Alembertian operator and additional terms depending on the nature of the velocity field. From such a wave equation, a corresponding parabolic equation can be derived for monochromatic sound waves. An exact equation for sound propagation in a homogeneous medium with a uniform velocity \mathbf{v} is [4]:

$$\left[\frac{\partial}{\partial t} + \mathbf{v} \cdot \nabla \right]^2 P(\mathbf{r}, t) = c^2 \Delta P(\mathbf{r}, t), \quad (1)$$

where $c = c(\mathbf{r})$ is the local sound speed, $P(\mathbf{r}, t)$ is the pressure acoustic field, Δ is the Laplacian operator and ∇ is the nabla operator. If the characteristic scale of velocity variations, L , is large in comparison with the acoustic wavelength λ , it is still reasonable to use equation (1) to evaluate the sound pressure field in the presence of a non uniform velocity. In the limit $\lambda/L \ll 1$ the operator $(\mathbf{v} \cdot \nabla)^2$ can be replaced by $v_i v_j \nabla_i \nabla_j$ (with the Einstein summation convention). For a monochromatic sound field $P'(\mathbf{r})$ equation (1) becomes [2]:

$$\left[\Delta + k^2 (1 + \epsilon) + 2ik \sqrt{1 + \epsilon} \frac{v_i}{c} \nabla_i + \frac{v_i v_j}{c^2} \nabla_i \nabla_j \right] P'(\mathbf{r}) = 0, \quad (2)$$

where $k = \omega/c_0$ (ω is the radian frequency of the sound source), $\epsilon = (c_0/c)^2 - 1$ is the variation of the standard refractive index, and $\nabla_i = \frac{\partial}{\partial x_i}$. The 0 subscripting variables correspond to constant mean values. When $\mathbf{v} = 0$, this equation reduces to the Helmholtz equation:

$$\left[\Delta + k^2 (1 + \epsilon) \right] P'(\mathbf{r}) = 0. \quad (3)$$

The additional terms in equation (2) compared to equation (3) contain the effects of the moving medium. The leading

term is $2ik\sqrt{1+\epsilon}\frac{v_i}{c}\nabla_i P'$. It is proportional to the Mach number and the spatial derivative of the pressure. Its maximum occurs when the direction of the sound wave is aligned with the velocity vector. This term represents the convection of the sound by the velocity field. The second additional term $\frac{v_i v_j}{c^2} \nabla_i \nabla_j P'$ is second order in Mach number and is proportional to the second spatial derivative of pressure. In inhomogeneous moving media, where both velocity and velocity gradients exist, the sound pressure field is the solution of the following equation [4]:

$$\left[\Delta + \underbrace{k^2(1+\epsilon)}_{(1)} - \underbrace{\left(\nabla \ln \frac{\rho}{\rho_0}\right) \cdot \nabla}_{(2)} + \underbrace{\frac{2ik}{c_0} \mathbf{v} \cdot \nabla}_{(3)} - \underbrace{\frac{2i}{\omega} \frac{\partial v_i}{\partial x_j} \frac{\partial^2}{\partial x_i \partial x_j}}_{(4)} \right] P'(\mathbf{r}) = 0. \quad (4)$$

When comparing with the Helmholtz equation (3), the new terms represent the wave scattering by dipoles through the wind terms (3) and by quadrupoles through the gradient terms (4). Therefore, for sound propagation through turbulence, this equation will describe more accurately scattering effects. The relative magnitude order of gradient terms (4) in equation equation (4) with respect to the wind term (3) is λ/L . In the following part of the paper we assume that the density ρ is uniform, so the term (2) disappears in equation equation (4). The previous wave equations were reduced to wide-angle parabolic equations by Ostashev *et al.* [1] and Dallois *et al.* [2]. The first step is to write the equation for forward propagation:

$$\left[\frac{\partial}{\partial x} - ik\sqrt{Q} \right] P' = 0. \quad (5)$$

From here, the \sqrt{Q} is simplified using a Padé approximation to yield:

$$\sqrt{Q} = \frac{1+p\mathcal{L}}{1+q\mathcal{L}}, \quad (6)$$

where $\mathcal{L} = Q - 1$, $p = 3/4$ and $q = 1/4$. Finally, representing P' in the form $P'(\mathbf{r}) = e^{ikx} \psi(\mathbf{r})$ we obtain the equations for the complex amplitude ψ . The numerical simulations presented in this paper deal with two dimensional (2D) geometries. If the procedure is applied to equation (2), the parabolic equation becomes (MW-WAPE, i.e. Mean Wind Wide Angle Parabolic Equation):

$$\left[1 + q\mathcal{F}_1 - ipk\mathcal{M}_1 - qk^2\mathcal{M}_1^2 \right] \frac{\partial \psi}{\partial x} = ik[(p-q)\mathcal{F}_1 + ik(p-q)\mathcal{M}_1 - iqk\mathcal{M}_1\mathcal{F}_1 + qk^2\mathcal{M}_1^2] \psi, \quad (7)$$

where:

$$\mathcal{F}_1 = \frac{1}{c^2 - v_x^2} \left[c_0^2 + 2i c_0 \frac{v_z}{k} \frac{\partial}{\partial z} + \frac{c^2 - v_z^2}{k^2} \frac{\partial^2}{\partial z^2} \right] - 1, \quad (8)$$

$$\mathcal{M}_1 = \frac{2v_x}{k(c^2 - v_x^2)} \left(ic_0 - \frac{v_z}{k} \frac{\partial}{\partial z} \right). \quad (9)$$

Similarly, if the procedure is applied to equation (4), the parabolic equation (TW-WAPE, i.e. Turbulent Wind Wide Angle Parabolic Equation) becomes:

$$\left[1 + q\mathcal{F}_2 - ipk\mathcal{M}_2 \right] \frac{\partial \psi}{\partial x} = ik[(p-q)\mathcal{F}_2 + ik(p-q)\mathcal{M}_2 - \frac{iq}{k}\mathcal{M}_2 \frac{\partial^2}{\partial z^2}] \psi, \quad (10)$$

where:

$$\mathcal{F}_2 = \epsilon + \frac{2i}{k} \frac{1}{c} \left(\frac{\partial v_x}{\partial x} + v_z \frac{\partial}{\partial z} \right) + \frac{1}{k^2} \left[1 + \frac{2i}{k} \frac{1}{c} \left(\frac{\partial v_x}{\partial x} - \frac{\partial v_z}{\partial z} \right) \right] \frac{\partial^2}{\partial z^2}, \quad (11)$$

$$\mathcal{M}_2 = \frac{2i}{k} \frac{v_x}{c} - \frac{2i}{k^3} \frac{1}{c} \left(\frac{\partial v_x}{\partial z} + \frac{\partial v_z}{\partial x} \right) \frac{\partial}{\partial z}. \quad (12)$$

We note that if all the velocities in equation (7) and equation (10) are zero, these equations reduce to the classical Padé(1,1) PE derived from the Helmholtz equation (3). In contrast to these wide-angle parabolic equations, we can produce a PE using only an effective index of refraction [5, 6]. In this case, the parabolic equation (WAPE, i.e. Wide Angle Parabolic Equation) becomes:

$$\left[1 + q\mathcal{L}_c \right] \frac{\partial \psi}{\partial x} = ik[(p-q)\mathcal{L}_c] \psi, \quad (13)$$

where:

$$\mathcal{L}_c = \epsilon_{eff} + \frac{1}{k^2} \frac{\partial^2}{\partial z^2} \quad (14)$$

with

$$\epsilon_{eff} = n_{eff}^2 - 1. \quad (15)$$

Here, $n_{eff}^2 = c_0^2/c_{eff}^2$, and c_{eff} is the effective sound speed. In this paper we report on a series of numerical experiments which compares sound propagation predicted from the standard PE using an effective index of refraction with sound propagation predicted from these two PEs (equation (7) and equation (10)) incorporating the velocity of the medium as additional vector terms (for simplicity note that in the following sections of the paper, the Turbulent Wind Wide Angle Parabolic Equation and the Mean Wind Wide Angle Parabolic Equation could be referred as “vector” PEs). In section 4 we study sound propagation through moving media without random fluctuations. In section 5 we compared sound propagation through turbulent velocity fields with sound propagation through turbulent temperature fields. We also simulate a velocity field having random spatial fluctuations over a range of length scales and could be suggestive of atmospheric turbulence. Celerity inhomogeneities are finally included to create an acoustic shadow zone and to study the sensitivity of the numerical simulations to the length scale of the dominant scattering random inhomogeneities.

3. Simulation of inhomogeneous “scalar” and “vector” random fields

The classical method of handling the propagation of waves through random media relies on a statistical approach. Starting from a parabolic approximation of the Helmholtz equation with a random refraction index, equations are deduced for the various statistical moments of the field: mean intensity, spatial coherence function, etc. . . However, to obtain equations in closed forms, a priori hypotheses have to be made about the correlation of the field (delta-correlation along the mean direction of propagation). To overcome these limitations we have suggested a different approach. We solve a deterministic wave equation for a series of realizations of simulated turbulent fields. Statistical results are then obtained through ensemble averaging. Currently, we generate the turbulence using a Time evolving Random Fourier Modes (TRFM) technique [7], such that the turbulent fluctuation at any point in the medium (either scalar or vector in nature) is calculated from the sum of a chosen number of modes. The RFM technique models the frozen turbulent fluctuations at any point in the medium from the sum of a limited number N of time-independent random Fourier modes. The mode orientations and phases are independent random variables chosen to yield homogeneous isotropic fields. The RFM technique has led to accurate quantitative predictions of average sound pressure level [8]. Most of the computations have been conducted in 2D, but some results are also available for the 3D case ([9] and [10]). Bailly *et al.* [7] added a time dependence and successfully applied the unfrozen RFM technique to the study of noise generation by turbulent flows. For atmospheric propagation studies, in which the statistical characteristics of the turbulence change with altitude [11], we seek to relax the homogeneity condition by allowing the modal amplitudes and the energy spectra that define them to vary with distance z from the ground plane. The random turbulent fields are horizontally stratified and *locally* isotropic and homogeneous in the stratum located at z , but the turbulence statistics vary from one stratum to the next [12]. We simulate the velocity at point \mathbf{r} as:

$$\mathbf{u}(\mathbf{r}, t) = 2 \sum_{n=1}^N \tilde{u}_n \cos[\mathbf{k}_n \cdot (\mathbf{r} - \mathbf{U}_c t) + \psi_n + \omega_n t] \boldsymbol{\sigma}_n. \quad (16)$$

To promote incompressibility the wave vector \mathbf{k}_n is normal to its associated Fourier contribution $\tilde{\mathbf{u}}_n$. A similar expression is used for temperature fluctuations:

$$T'(\mathbf{r}, t) = \sum_{n=1}^N \tilde{T}_n \cos[\mathbf{k}_n \cdot (\mathbf{r} - \mathbf{U}_c t) + \phi_n + \omega_n t]. \quad (17)$$

Figure 1 illustrates the spectral description of a 2D Fourier velocity mode. In generating a two-dimensional field, the orientation of the wave vector \mathbf{k}_n is fixed by the angle θ_n . In the case of the velocity, the unit vector $\boldsymbol{\sigma}_n$ is determined

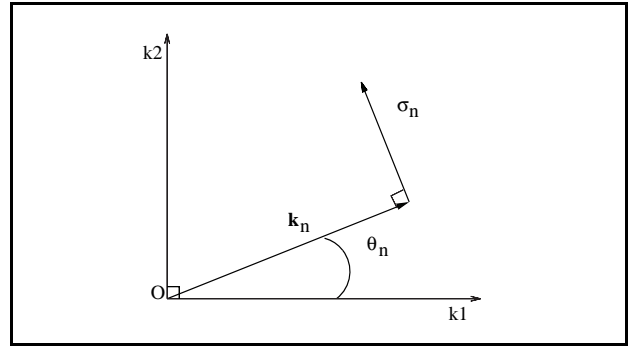


Figure 1. Sketch of the geometry for the n th Fourier random mode. The orientation of the wave vector \mathbf{k}_n is fixed by the angle θ_n and the unit vector $\boldsymbol{\sigma}_n$ is perpendicular to the wave vector \mathbf{k}_n .

from θ_n : $\boldsymbol{\sigma}_n = -\sin(\theta_n)\mathbf{e}_r + \cos(\theta_n)\mathbf{e}_z$. \mathbf{e}_r and \mathbf{e}_z are unit vectors in the r and z directions, respectively. Local isotropy and homogeneity in 2D is obtained by selecting three random variables θ_n , ψ_n and ϕ_n from independent uniform p.d.f between 0 and 2π . The modal amplitude \tilde{u}_n is such that:

$$\tilde{u}_n = \sqrt{E(k_n; z)\Delta k_n} \quad \text{with } k_n = |\mathbf{k}_n|. \quad (18)$$

$E(k_n; z)$ is the altitude-dependent 2D kinetic energy spectrum, which is approximated by a von Karman expression:

$$E(k; z) = \frac{8}{9} \frac{\sigma_u^2(z)}{k_e} \frac{(k/k_e)^3}{\left[1 + (k/k_e)^2\right]^{14/6}} \times \exp\left[-2\left(\frac{k}{k_\eta}\right)^2\right] \quad (19)$$

with $k_e = 0.586/L_i(z)$. The velocity variance $\sigma_u^2(z)$ and integral length scale $L_i(z)$ vary with altitude z , and k_η is the Kolmogorov wavenumber. For temperature, the modal amplitude \tilde{T}_n is such that:

$$\tilde{T}_n = \sqrt{G(k_n; z)\Delta k_n} \quad \text{with } k_n = |\mathbf{k}_n|. \quad (20)$$

$G(k_n; z)$ is the altitude-dependent 2D spectrum, which is approximated by a von Karman expression:

$$G(k; z) = \frac{5}{3} \frac{\sigma_T^2(z)}{L_o(z)^{5/3}} \left(k^2 + \frac{1}{L_o(z)^2}\right)^{-11/6} \times \exp\left[-\left(\frac{k}{k_m}\right)^2\right] \quad (21)$$

with $k_m = 5.92/l_o$. The temperature variance $\sigma_T^2(z)$ and outer turbulent length scale $L_o(z)$ vary with altitude z , and l_o is the inner turbulent scale. The temporal evolution of each mode is governed by the convection of the turbulence by the mean flow \mathbf{U}_c , and a circular frequency ω_n , which is based on a large scale sweeping time. This frequency is a random variable whose mean value is related to the wave number through the Heisenberg formula:

$\omega_o = k \cdot u'$ where u' is the rms value of the velocity fluctuations; the p.d.f. of ω_n is chosen as a Gaussian according to: $g(\omega) = 1/\omega_o \sqrt{2\pi} \exp\left(-(\omega - \omega_o)^2/2\omega_o^2\right)$. Recently, Juvé *et al.* [13] introduced Large Eddy Simulations (LES), when examining propagation through a temporally evolving medium. In LES only the largest, most energetic scales of the flow are resolved via filtered Navier-Stokes equations; the cutoff wavenumber k_c defining the smallest resolvable scales is determined by the grid spacing. The effects of unresolved scales ($k > k_c$) are incorporated via a subgrid closure model, but at present no acoustic modelling exists for including these subgrid scales in propagation calculations. To ensure that our field-generation technique produced reasonable results, we used an ensemble of 5000 velocity fields corresponding to the experimental data of Comte-Bellot and Corrsin [14]. From this ensemble we calculated the first four single-point moments for the three components of the velocity and the nine components of velocity derivative (for details see [10] and *et al.* [15]). Our technique compares favorably with the experiment of Comte-Bellot and Corrsin. In the case of temperature fields our modelling technique is in good agreement with experimental data obtained in a large anechoic chamber in Ecole Centrale de Lyon [16]. One of the advantage of this modelling technique is its ability to generate random fields with prescribed spectra. In addition, since the random fields have been modelled in terms of a fixed number of discrete Fourier modes, we can derive analytically the fields and their spatial derivatives at every point of the physical space. The index of refraction n is then expressed in terms of a mean part $n = c_0/c$ and a fluctuating part $\mu = -T'/2T_0 - \mathbf{u} \cdot \boldsymbol{\nu}$, where $\boldsymbol{\nu}$ is the direction of propagation of the acoustic wave (in this paper the vector $\boldsymbol{\nu}$ correspond to the horizontal axis and $\mathbf{u} \cdot \boldsymbol{\nu} = v_x$).

4. Sound propagation in a moving atmosphere

In this section we compare differences in predictions of sound transmission losses derived from the use of equation (13) based on the approximation of the effective sound speed c_{eff} and correct wide-angle parabolic equations equation (7) and equation (10). First we present numerical simulations that validate the numerical schemes of solving new parabolic equations (equation (7) and equation (10)) by comparing integrations of WAPE (equation (13)), MW-WAPE (equation (7)) and TW-WAPE (equation (10)) with known solutions. Second we carry out a series of numerical experiments in which we compare results of TW-WAPE vs. WAPE and MW-WAPE vs. WAPE, depending on the moving medium. In all cases, we restrict ourselves to two-dimensionnal problems which are representative of outdoor sound propagation. We consider the two-dimensional propagation of sound from a point source located at $x = 0$ and $z = h_s$ (see Figure 2). Numerically, each of previous parabolic equations (equation (7), equation (10) and equation (13)) is discretized on a uniform mesh ($i \Delta x, j \Delta z$) using a standard finite difference method. z -derivatives are evaluated with centered difference approximations, and Crank-Nicholson scheme is implemented as a

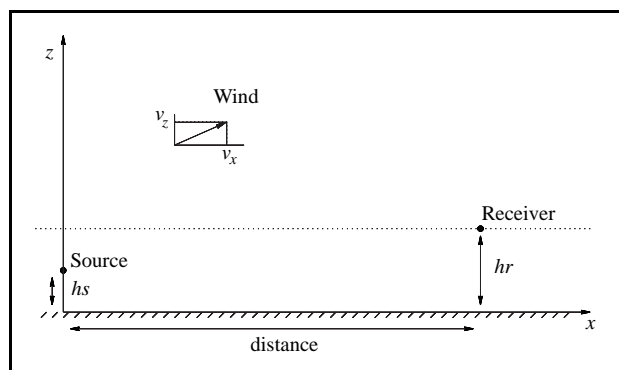


Figure 2. Geometry of the two-dimensional problem.

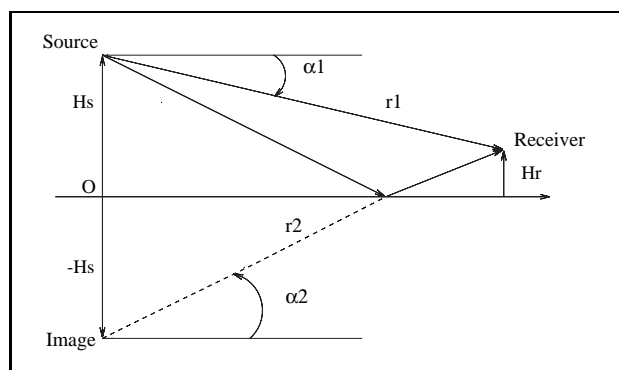


Figure 3. The geometry of the problem which includes the image source.

marching algorithm. The horizontal step Δx and the vertical step Δz are much smaller than the sound wavelength λ . Typically $\Delta x, \Delta z$ are $0.1 - 0.2\lambda$. The ground is modelled as a perfectly reflecting plane by introducing a source at $z = h_s$ and its image at $z = -h_s$. The source is initialized by a Gaussian starter. A non reflecting boundary condition is imposed at the top of the computational domain by adding an absorbing layer of several wavelength thickness (see [3]).

4.1. Validation and comparison with an analytical solution

In order to validate the sound pressure levels predicted by the use of new PEs (equation (7) and equation (10)), we consider a simple model of a moving atmosphere in which the wind velocity vector is constant and parallel to the horizontal axis (i.e. $v_x = v, v_z = 0$). In the presence of a perfectly reflecting plane boundary, it is possible to evaluate the sound pressure field using the method of image source (see Figure 3). Using the analytical solution of Ostashev [4], we obtained:

$$P(\mathbf{r}) = \sum_{j=1}^2 \frac{1}{\sqrt{r_j}} \exp \left[ik_0 r_j \frac{M \cos \alpha_j}{M^2 - 1} - ik_0 r_j \frac{\sqrt{1 - M^2 \sin^2 \alpha_j}}{M^2 - 1} \right] \quad (22)$$

where $j = 1$ and $j = 2$ correspond to the source and its image, respectively, α is the angle between the horizontal axis and the line-segment connecting source and receiver, and r_j is the distance between the receiver and the source or its image. Note that in this solution, the phase is calculated to any order of the Mach number M to preserve possible changes in the interference pattern due to the effects of the wind velocity.

In Figure 4 we compare the transmission loss evaluated with the PEs equation (7) and equation (10) to the transmission loss given by the analytical solution equation (22). Note that the relative acoustic pressure level is defined as $20 \log_{10} \sqrt{r} \sqrt{\langle P' P'^* \rangle} / |P'_0|$ where r is the distance between the source and the receiver, P'_0 is the reference pressure at one meter from the source in free space and $\langle P' P'^* \rangle$ is the mean square of the acoustic pressure. The horizontal velocity is constant and equal to 10 ms^{-1} . The acoustic frequency is $\nu = 340 \text{ Hz}$. The vertical positions of the source and the receiver are: $h_s = 5 \text{ m}$ and $h_r = 5 \text{ m}$. The agreement between the analytical and new parabolic solutions is excellent.

Figure 5 presents the results obtained with the new PE's equation (7) and equation (10) and the standard PE equation (13). The sound frequency ν is 680 Hz , the wind velocity vector is parallel to the x axis, $v_x = 20 \text{ ms}^{-1}$ and $v_z = 0 \text{ ms}^{-1}$. The height of the source is 5 m and the receiver is located at 10 m from the ground. As expected, the prediction obtained with the standard parabolic equation equation (13) is different from the two other predictions based on the new parabolic equations. This difference increases with the distance of propagation. In terms of geometric acoustics, the receiver is reached by two different paths: a direct ray and a reflected ray. The sound speed, $c + v \cos \theta$, varies on each ray with θ and the use of the effective sound speed, $c + v_x$, introduces a cumulative phase error in standard parabolic equation. This error increases with the receiver height, the distance of propagation and the wind velocity.

4.2. Effects of a mean vertical wind gradient

Now we consider the sound propagation in an inhomogeneous medium with a constant vertical wind gradient dv_x/dz . The wind profile is the linear wind profile used in [17]: $v_x = 0.1 \cdot z$ for $z < 200 \text{ m}$, $v_x = 20 \text{ m.s}^{-1}$ for $z > 200 \text{ m}$, and $v_z = 0$. This downward propagation geometry is very sensitive to the wind velocity. First, for long distances, because of the occurrence of caustics, when more than two rays reach the receiver. Secondly, the paths are curved downward so directions of sound propagation differ from the horizontal axis.

In Figure 6 we compare the transmission losses obtained with the standard PE (equation (13)) and new wide-angle PE (equation (10)) for three different heights of the receiver ($h_r = 5 \text{ m}$, 10 m , 50 m). We present results for a frequency $\nu = 680 \text{ Hz}$. We notice significant differences between two predictions. Again, as expected the difference depends on the receiver height and the distance of propagation. For example with a receiver located at the altitude of 50 m when the

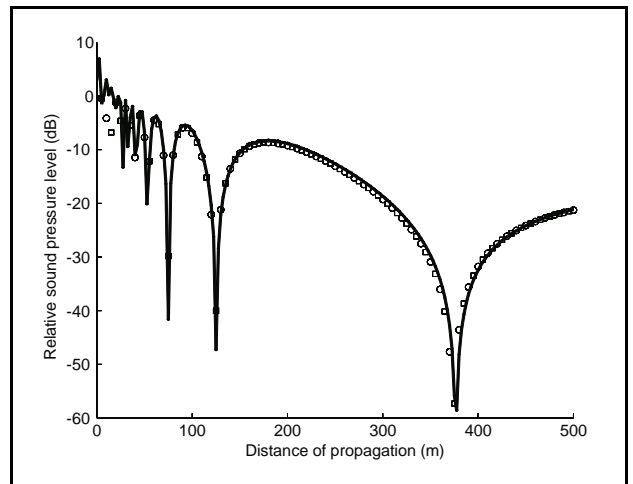


Figure 4. Comparison between analytical solution and the results obtained with new parabolic equations: [□] equation (7), [○] equation (10). The horizontal velocity is constant and equal to 10 ms^{-1} . $\nu = 340 \text{ Hz}$, $h_s = 5 \text{ m}$ and $h_r = 5 \text{ m}$.

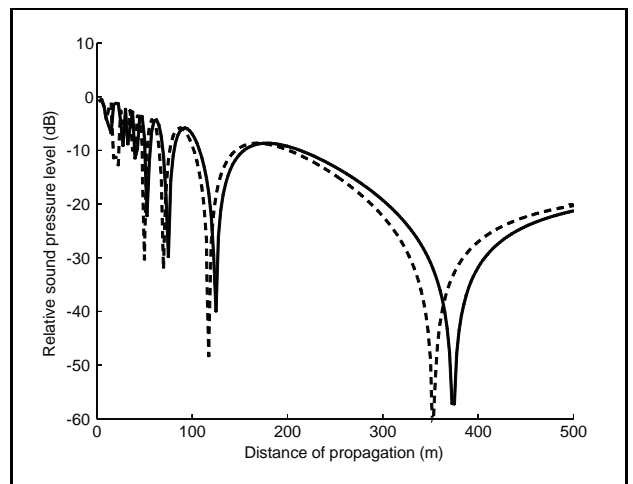


Figure 5. Acoustic pressure level versus distance of propagation: (---) WAPE results, (—) MW-WAPE and TW-WAPE results. Uniform horizontal velocity field: $\mathbf{v} = v_x = 20 \text{ ms}^{-1}$, $\nu = 680 \text{ Hz}$, $h_s = 5 \text{ m}$ and $h_r = 10 \text{ m}$.

distance of propagation is greater than 1000 m , the positions of interference maxima and minima are totally shifted and the difference in the transmission loss level is of the order of 5 dB . For large distances (here $r > 1000 \text{ m}$), a shift appears between the interference patterns of the WAPE and MW-WAPE results. As in the previous case, the motion effects progressively increase with the distance of propagation. These effects are more important for the higher elevation when the direction of propagation significantly differs from the horizontal axis. For a propagation distance of 2 km , the displacement of the interference location is about 40 m at $z = 10 \text{ m}$ and about 120 m at $z = 50 \text{ m}$ and the difference in the acoustic pressure level is respectively 5 dB and 10 dB . As expected in the WAPE predictions the phase errors in the sound field dramatically increase with range.

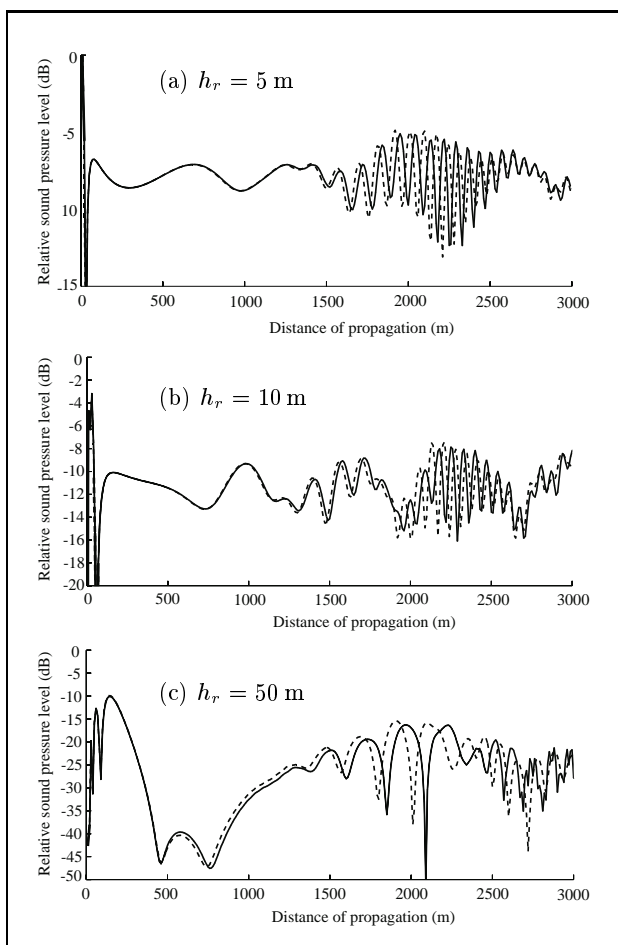


Figure 6. Acoustic pressure level versus distance of propagation: (—) WAPE results, (—) MW-WAPE results. Horizontal velocity field: $\mathbf{v} = v_x(z) = 0.1z \text{ ms}^{-1}$. Parameters: $\nu = 680 \text{ Hz}$, $h_s = 5 \text{ m}$ and $h_r = 5 \text{ m}, 10 \text{ m}$ or 50 m .

4.3. Effects of a mean vertical wind

We consider the sound propagation in an inhomogeneous medium with a constant vertical wind, $v_x = 0$ and $v_z = v$. In Figure 7 we compare predictions of the transmission losses using three PEs. The frequency of the source is $\nu = 400 \text{ Hz}$. The heights of the source and receiver are $h_s = 5 \text{ m}$ and $h_r = 10 \text{ m}$, respectively. As expected, standard PE (equation (13)) does not take into account the vertical wind velocity and the phase errors in the sound field dramatically increase with range. For example at a distance of 240 m the use of standard PE equation (13) results in destructive interference while new PEs equation (7) and equation (10) do not reveal it. We also plotted on Figure 7 the transmission losses calculated using a ray tracing algorithm. There is a concern whether the geometric acoustics method is able to include the velocity vector in exact way [10]. One of the difficulties of this method is related to the finding out of all eigenrays, which are necessary for computation of the transmission losses. Of course, this approach will fail in a shadow zone. Nevertheless up to a distance of propagation of 200 m , the comparison is in favor of new PEs which rigorously incorporate the wind velocity.

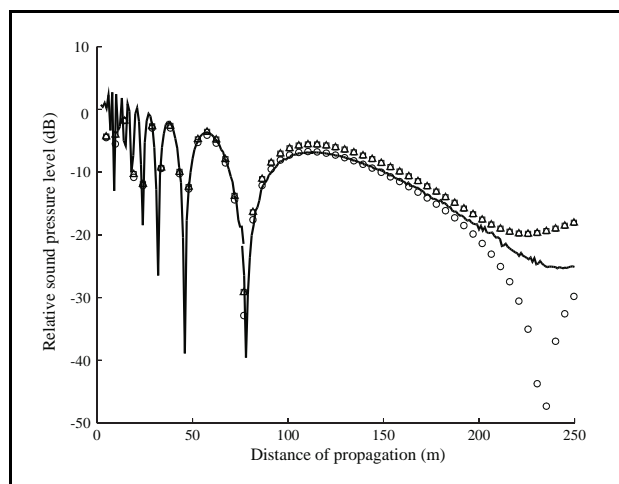


Figure 7. Comparison between results obtained by the ray tracing program [—], the TW-WAPE equation (10) [Δ] and MW-WAPE equation (7) [\square]. Standard WAPE equation (13) solution is plotted with [\circ]. The vertical velocity is constant and equal to $v_z = 5 \text{ ms}^{-1}$. $\nu = 400 \text{ Hz}$, $h_s = 5 \text{ m}$ and $h_r = 10 \text{ m}$.

5. Sound scattering in a shadow zone by turbulence

We consider now the propagation of acoustic waves in an upward-refracting atmosphere. For outdoor sound propagation near the ground, the combined effects of air temperature and wind speed typically produce an effective sound speed that decreases with altitude. This has the effect of bending sound upwards such that a deterministic shadow zone appears at a short distance from a near-ground source. For a receiver located in this region there is no direct ray coming from the source; sound energy can only penetrate the shadow zone due to diffraction and turbulent scattering. In a first series of numerical experiments, using the standard “scalar” wide-angle parabolic equation (WAPE) we examine the influence of scale resolution on numerical simulation of long range sound propagation through the atmosphere. Specifically, we seek to answer the questions: How does the inclusion/exclusion of turbulent field statistical inhomogeneity affect our results, what portion of the \mathbf{u} and T' spectra must be adequately resolved, and, given the current limitations on grid size (k_c), is the LES approach alone viable for atmospheric propagation simulations? The objective of the second series of numerical simulations is to determine the benefit of using a more accurate “vector” wide-angle parabolic equation (TW-WAPE) in determining acoustic propagation in moving media.

5.1. Modelling of an upward-refracting turbulent atmosphere

Our inputs to the propagation model were as follows. The mean sound speed profile, was calculated from [18]:

$$c(z) = \begin{cases} c_0 - A \ln(z/d) & z \geq z_0 \\ c_0 - A \ln(z_0/d) & z < z_0 \end{cases} \quad (23)$$

where $c_0 = 340$ m/s, $z_0 = 0.01$ m, $A = 2$ m/s and $d = 6 \times 10^{-3}$ m. When random inhomogeneities, either vector or scalar, are added to a sound speed field that generates a shadow zone, acoustic pressure will leak into this zone through scattering [19]. We assume that the time variation of the turbulent medium is much greater than the acoustic travel time between the source and receiver. So the turbulent medium is considered as frozen. However, we are interested in a velocity field that is consistent with that of an atmospheric boundary layer above a rigid surface, i.e. one whose energy spectrum depends on height z . Several models have been proposed for this height dependency — B. A. Kader and A. M. Yaglom [20], S. Khanna [21] and D. K. Wilson *et al.* [22]. Scaling of the surface layer is normally based on the premise that the turbulence structure depends entirely on the surface Reynolds stress τ , the surface heat flux Q , and the buoyance $\beta = g/T_s$, where g is the gravitational acceleration, and T_s is the surface temperature. From these parameters one can derive representative scales for velocity $u_* = \sqrt{\tau/\rho}$, where ρ is density, temperature $T_* = -Q/u_*$, and length $L_{mo} = -u_*^3/\beta Q$. Like the temperature scale T_* , the Monin-Obukhov length L_{mo} is negative when the ground is being heated (statically unstable condition as on a sunny day) and positive when the ground is cooling (statically stable condition as on a clear night). In this paper we only consider the former case, $T_* < 0$. We adopt the Kader and Yaglom model which divides the boundary layer into three sublayers according to the dimensionless vertical scale $\eta = z/L_{mo}$. The normalized altitude $\zeta = z/L_{mo}$ represents the ratio of buoyant to inertial forces acting in the surface layer. For the standard deviation of the temperature we have:

$$\sigma_T = \begin{cases} -2.9T_* & 0 < -\zeta < 0.1 \\ -1.4T_* (-\zeta)^{-1/3} & 0.3 < -\zeta < 3 \\ -1.5T_* (-\zeta)^{-1/3} & 5 < -\zeta \end{cases} \quad (24)$$

For the standard deviation of the wind (velocity), we can make use of the relations for only one component (horizontal longitudinal, horizontal lateral, or vertical) because our modified RFM scheme is based on an isotropic formulation. We opt for the horizontal longitudinal component (in the direction of the mean wind) and note that the longitudinal and lateral components differ by less than 10%. We have:

$$\sigma_u = \begin{cases} 2.7u_* & 0 < -\zeta < 0.1 \\ 1.7u_* (-\zeta)^{-1/3} & 0.3 < -\zeta < 3 \\ 0.7u_* (-\zeta)^{-1/3} & 5 < -\zeta \end{cases} \quad (25)$$

As with the wind components, the isotropy of the model forces us to select a single integral scale. We select the relations for the horizontal scale:

$$L_i = \begin{cases} z/\kappa^2 & 0 < -\zeta < 0.1 \\ \kappa_{fc}^2 (-\zeta)^{-2/3} z & 0.3 < -\zeta < 3 \\ z/\kappa_{fc}^2 & 5 < -\zeta \end{cases} \quad (26)$$

$\kappa = 0.4$ is the von Kármán's constant, and $\kappa_{fc} = 1.2$. For further details regarding turbulence modelling, refer to

[11]. For the RFM turbulence model, we logarithmically distributed 400 modes between 10^{-3} m^{-1} and 10^3 m^{-1} . A Kolmogorov microscale of 5 mm was assumed for the inner turbulent length scale. The altitude-dependent outer turbulence scale and variances were calculated for: $u_* = 0.6$ m/s, $T_* = -0.4$ K, $L_{mo} = -26$ m, $\mathbf{U}_c = 0$ m/s \mathbf{e}_r , $\sigma_u = 1$ m/s. Means were calculated by ensemble averaging over twenty realizations.

5.2. Wind velocity versus temperature fluctuations

The scattering properties of a vectorial random medium are different from those of a scalar medium [23] [4]. In considering sound propagation through an upward-refracting turbulent atmosphere, Juvé *et al.* [24] compared the pressure fields for a scalar and vectorial case using the same variance of the fluctuations, the same integral scale and gaussian correlation functions. The authors found that, relative to the scalar case, scattering was more intense for the vectorial fluctuations, which produced a 10-12 dB greater mean relative sound pressure level (SPL) in the shadow zone. We now compare the results obtained with our inhomogeneous “scalar” and “vector” random fields. The velocity and temperature fluctuations were generated using the technique outlined previously using the same variance and the same integral scale.

Figure 8 presents the results obtained with the standard PE (equation (13)). We consider two frequencies $\nu = 424Hz$ and $\nu = 828Hz$. The height of the source is 3.7 m and the receiver is located at the same altitude. The difference in mean relative sound pressure level (SPL) in the shadow zone is much greater than 25 dB. Since the variances and outer length scales are the same order of magnitude, this is attributed to the behavior of the energy spectra, equations 21 and 19, in the inertial subrange. As wavenumber increases, the energy in the inertial range of the temperature spectrum decreases as $k^{-8/3}$ while for the kinetic energy spectrum the decrease is much slower, $k^{-5/3}$. Thus, for the range of scales that most influences scattering into the shadow zone, the velocity fluctuations are significantly more energetic. This suggests that scattering by wind velocity fluctuations is the dominant mechanism allowing acoustical energy to penetrate the shadow zone. The results presented in the remaining sections pertain to scattering by turbulent velocity fluctuations.

5.3. Effects of the wavenumber cutoff k_c

Using the inhomogeneous turbulence model, calculations were performed to determine the sensitivity of our results to the cutoff wavenumber k_c . Figure 9 presents the results obtained with the standard PE equation (13). Normally, the largest wavenumber considered in the calculations was $k_c = 10^3 \text{ m}^{-1}$, which allowed us to resolve eddies down to the Kolmogorov microscale, 5 mm. We now consider four cases for which $k_c = 10 \text{ m}^{-1}$, 5 m^{-1} , 1 m^{-1} , and 0.4 m^{-1} . We accomplished this by removing modes having $k > k_c$ from the respective calculations. This is the *only* difference between the cases; all other factors (mode amplitudes and orientations, variances, length scales, *etc.*) were the same.

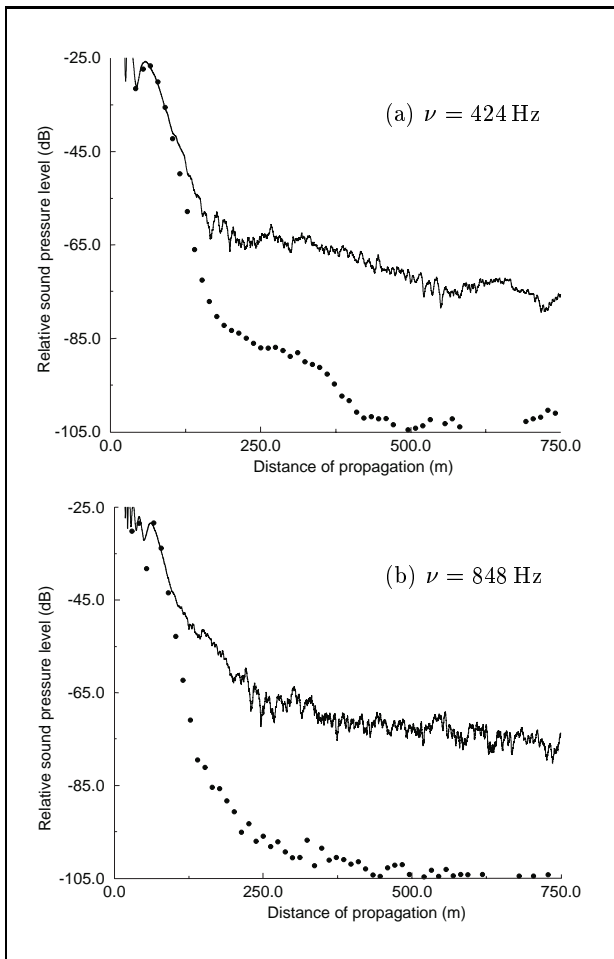


Figure 8. Mean relative sound pressure level due to temperature (●) and wind velocity (—) fluctuations. $h_s = h_r = 3.7$ m.

Figure 9 shows how decreasing k_c (neglecting the smaller eddies that comprise the spectrum) reduces the predicted SPL in the shadow zone. For 424 Hz one can neglect wavenumbers larger than 5 m^{-1} , and for 848 Hz one can neglect wavenumbers larger than 10 m^{-1} . These roughly correspond to eddies of size 1.2 m and 0.6 m, respectively, and define the lower bound of the range of sizes principally responsible for scattering into the shadow zone. A reasonable estimate for these values can be calculated from the Bragg's relation $\lambda = 2L \sin(\theta/2)$ which states that turbulent eddies of size L scatter sound of wavelength λ through the angle θ . The wavenumbers $2\pi/L$ of the eddies scattering through this angle θ (about 10°) are 1.5 m^{-1} and 3 m^{-1} for 424 Hz and 848 Hz, respectively. But these "critical" k_c are significantly larger than the cutoff wavenumbers currently achieved by LES simulations of the atmospheric boundary layer. Even using an embedded fine mesh near the ground, the vertical grid spacings are at least 10 m, an order of magnitude larger than the dominant scattering inhomogeneities.

5.4. TW-WAPE simulation versus WAPE simulation

In the numerical experiments which follow, we report on both individual and ensemble results. In the individual cases, we

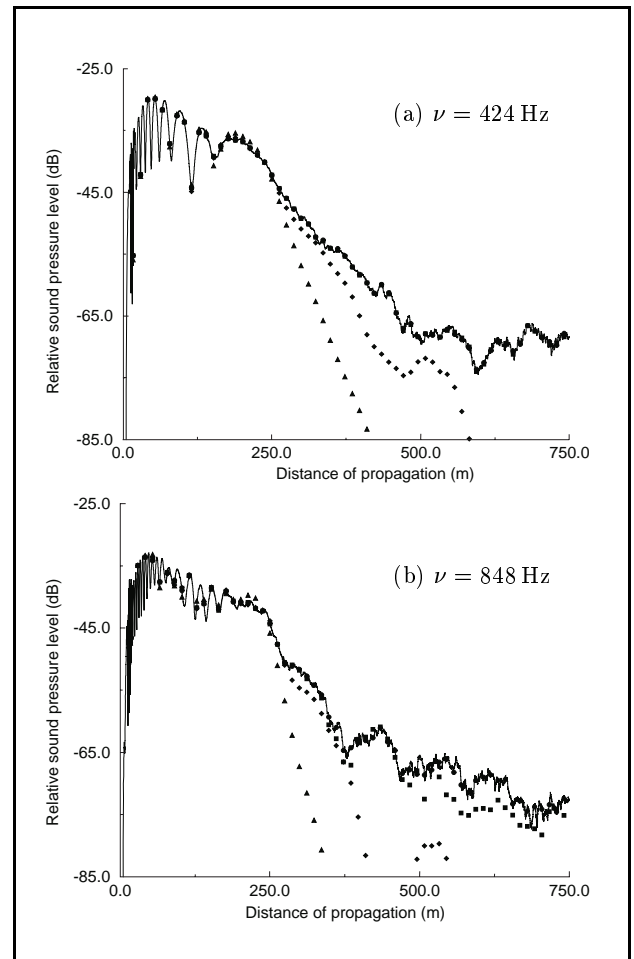


Figure 9. Mean relative sound pressure level (SPL): Comparison between a cutoff wavenumber of 10^3 m^{-1} (solid line —), 10 m^{-1} (solid ●), 5 m^{-1} (solid □), 1 m^{-1} (solid ◇), and 0.4 m^{-1} (solid △). In both cases $h_s = 25$ m and $h_r = 3.7$ m.

calculate acoustic propagation through a single realization of the velocity field. In the ensemble cases, we report on averages taken over 20 realizations (for the average sound pressure a fast convergence of the results is obtained with a relatively small number of realizations [8] and for higher statistics a detailed analysis can be found in [9] and [3] where different probability distributions have been pointed out depending on the scattering regime).

Figure 10 compares the relative pressure level of the WAPE integration and the TW-WAPE integration at two different frequencies for the inhomogeneous turbulent velocity. The frequency of the source is $\nu = 340$ Hz and $\nu = 170$ Hz. The source is $h_s = 5$ m above the ground. The receiver is $h_r = 10$ m above the ground. The dashed lines are the WAPE results and the solid lines are the TW-WAPE results. The graphs display only the shadow zone region. The difference between the two curves (WAPE and TW-WAPE) varies between 1 or 2 dB for the $\nu = 340$ Hz case and between 3 or 4 dB for the $\nu = 170$ Hz case. For lower frequencies, the differences are increasing. It would appear that in the sub-layer model, the vector terms in TW-WAPE make significant contributions.

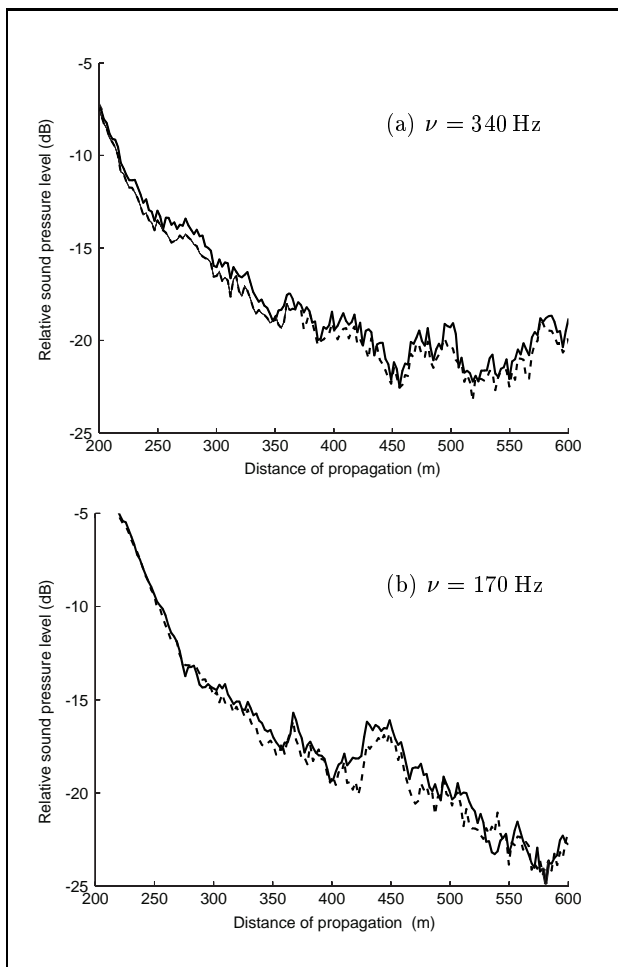


Figure 10. Ensemble average of relative acoustic pressure level versus distance of propagation for inhomogeneous turbulent fields: (—) WAPE results and (—) TW-WAPE results. Inhomogeneous turbulence parameters: $L_{mo} = -26$ m and $u_* = 0.6$ ms⁻¹. $h_s = 5$ m and $h_r = 10$ m.

An interesting observation is that, even if the average values of the pressure field are close, single realizations can differ between the WAPE integration and the TW-WAPE integration. Figure 11 presents relative acoustic pressure level for a single realization of an inhomogeneous turbulent velocity field. Two frequencies are investigated: $\nu = 340$ Hz (upper) and 170 Hz (lower). The receiver height is $h_r = 10$ m. The same realization of the turbulent field is used in both cases, and the two figures show differences between the WAPE (dashed line) and TW-WAPE (solid line) solutions. Again the differences are greater for low frequencies. It is remarkable that for the same realization, the behaviour of the acoustic field could be so different from one frequency to the next. So, even if mean results are not greatly affected by the use of the TW-WAPE, single realisations are (cf. Figure 11, Figure 12). And, on Figure 12 we clearly note the influence of the vertical position of the receiver. Finally we consider vertical relative pressure level in the shadow zone (cf. Figure 13) for a single realisation. The left curves correspond to a distance of propagation $x = 400$ m and the right curves to a distance of propagation $x = 600$ m. The solid line represents the

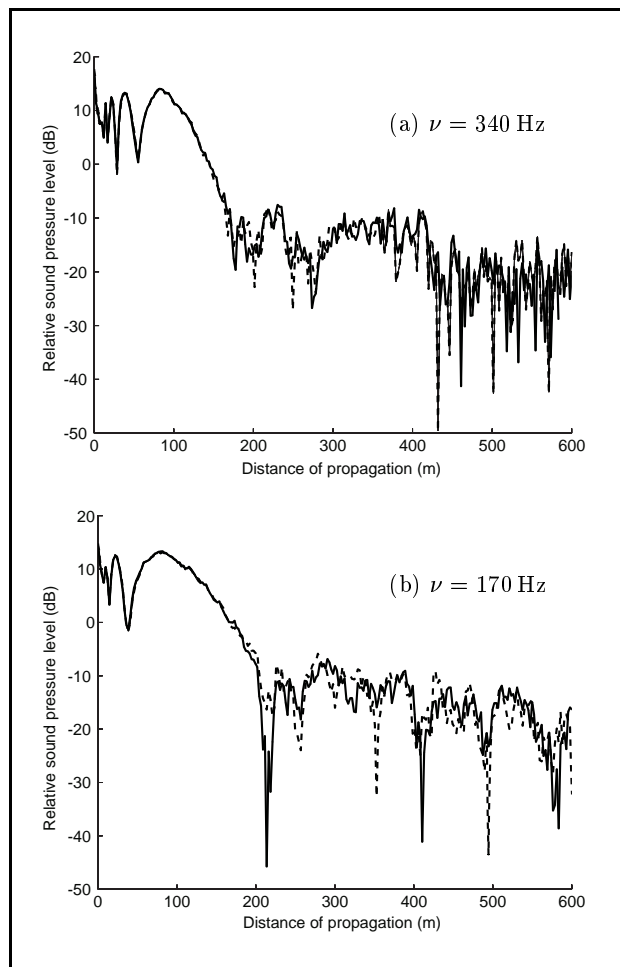


Figure 11. Relative acoustic pressure level versus distance of propagation for inhomogeneous turbulent fields: (—) WAPE results and (—) TW-WAPE results. Inhomogeneous turbulence parameters: $L_{mo} = -26$ m and $u_* = 0.6$ ms⁻¹. $\nu = 170$ Hz, $h_s = 5$ m, $A = 2$ ms⁻¹, $d = 10^{-3}$ m.

TW-WAPE results and the dashed line, the WAPE results. First, we note that for altitudes greater than 20 m, there is little difference between the “scalar” PE and the “vector” PE. In the layer close to the ground ($z < 20$ m) the difference is significant. This difference increases with the distance of propagation (more details are available in [25]).

6. Conclusion

In this paper we have presented 2D numerical simulations of sound propagation and scattering in random moving media. We have shown that the use of the effective sound speed assumption is not sufficient to describe accurately the effects of mean and random wind velocity on sound propagation through moving media. To summarize we considered two wide-angle “vector” PEs designed to provide for the calculation of long range sound propagation in moving media: the MW-WAPE and the TW-WAPE. Their derivations and conversions to numerical codes were validated by comparing results from a numerical experiment with an analytic solution.

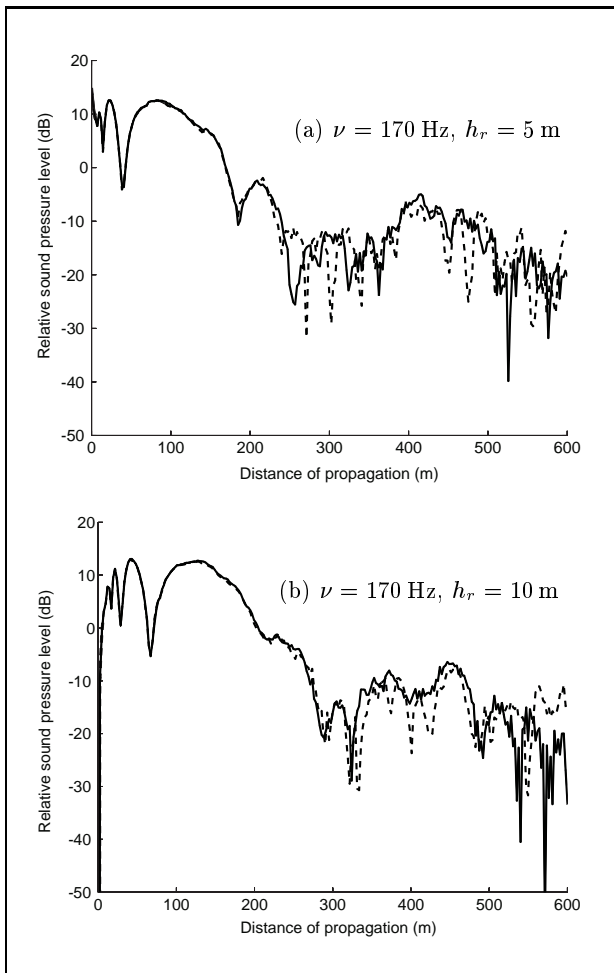


Figure 12. Relative acoustic pressure level as a function of the distance of propagation for $\nu = 170$ Hz and two receivers $h_r = 5$ m and $h_r = 10$ m: (---) WAPE single realization results and (—) TW-WAPE single realization results. Inhomogeneous turbulence parameters: $L_{mo} = -26$ m and $u_* = 0.6$ ms $^{-1}$. $\nu = 170$ Hz, $h_s = 5$ m, $A = 2$ ms $^{-1}$, $d = 10^{-3}$ m.

The MW-WAPE is used to predict sound wave propagation in the presence of a mean wind which is not colinear to the direction of propagation. The TW-WAPE is used when scattering by a turbulent velocity field is considered. A series of numerical experiments were then conducted on several classes of two-dimensional inhomogeneous media with rigid lower boundaries to evaluate the efficacy of these “vector” PEs vis-a-vis the traditional “scalar” PE.

At large distances of propagation and from an ensemble of statistically similar experiments, average interference patterns obtained from the MW-WAPE are measurably different than those obtained from the “scalar” WAPE. The cumulative effect of more accurately representing acoustic phase seems to become important. The standard PE is not accurate to treat the effect of the mean wind on sound propagation. And since the difference between scalar and vector representations of velocity effects would be more pronounced in a three-dimensional case, it would appear that using the more complicated MW-WAPE in lieu of the simpler WAPE is justified. Obviously, MW-WAPE equation should be used to

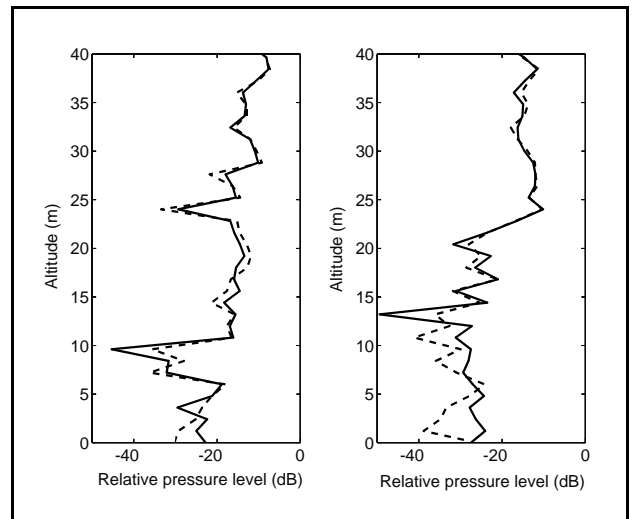


Figure 13. Relative acoustic pressure level as a function of the altitude along a vertical line for $x = 400$ m (left) and $x = 600$ m (right): (---) WAPE single realization results and (—) TW-WAPE single realization results. Inhomogeneous turbulence parameters: $L_{mo} = -26$ m and $u_* = 0.6$ ms $^{-1}$. $\nu = 170$ Hz, $h_s = 5$ m, $A = 2$ ms $^{-1}$, $d = 10^{-3}$ m.

compute the effects of a mean cross wind component v_y on sound propagation near the ground. On the other hand, ensemble numerical experiments using the TW-WAPE did not display significant differences from those using the WAPE—at least on average. However, when results were compared for individual experiments, significant differences appeared. The TW-WAPE will be tested in more complex geometrical configurations created by the presence of an acoustic barrier along the sound wave path. In this case, especially behind the barrier the scattering of sound is affected by all the components of the wind vector and the associated gradients.

We also presented a technique for generating inhomogeneous “scalar” and “vectorial” random fields, allowing us to simulate the effects of altitude-dependent atmospheric turbulence statistics. We began by examining the relative importance of scattering by wind and temperature fluctuations. For the assumed wavenumber dependence of the temperature and kinetic energy spectra in the inertial subrange, wind speed fluctuation is the dominant factor causing acoustical energy to penetrate the shadow zone. Next we examined the importance of spatial-frequency cut-off of the turbulent field, this allow us to make clear what resolution is really needed for atmospheric propagation studies. A reasonable estimate for these values can be predicted from the Bragg relation. Because the eddies responsible for scattering into the shadow zone are an order of magnitude smaller than current grid sizes, LES is not by itself a viable turbulence model for simulations of sound propagation from near-ground sources in an upward-refracting atmosphere. It should, however, be possible to develop an LES-RFM hybrid in which RFM is used to fill in the subgrid scales.

The observations and interpretations in this paper were for two-dimensional propagation. As noted above, a scalar representation of the velocity effects may be marginally adequate

in two-dimensions, but in three-dimensions a vector representation will surely be necessary. Especially in the case of multiscale velocity fluctuations, interference and scattering are very sensitive to acoustic frequency, which would suggest that wide-angle parabolic equations must be used—at least over long propagation distances.

Acknowledgement

This work is based on a collaborative CNRS/NSF grant and an IDRIS project No. 990742. The authors would like to thank Dr. V. Ostashev for his interest in this work while he was a Visiting Professor at Ecole Centrale de Lyon.

References

- [1] V. Ostashev, D. Juvé, P. Blanc-Benon: Derivation of a wide-angle parabolic equation for sound waves in inhomogeneous moving media. *Acustica united with Acta Acustica* **83**(3) (1997) 455–460.
- [2] L. Dallois, P. Blanc-Benon, D. Juvé, V. Ostashev: A wide angle parabolic equation for sound waves in moving media. Proc. Eighth International Symposium on Long Range Sound Propagation, Applied Research Lab, The Pennsylvania State University, 1998. 194–208.
- [3] L. Dallois: Propagation des ondes acoustiques dans les milieux en mouvement : extension grand angle de l'approximation parabolique. Dissertation. Ecole Centrale de Lyon, ECL, n° 2000-37, 2000.
- [4] V. Ostashev: Acoustic in moving inhomogeneous media. E & FN SPON, London, 1997.
- [5] K. Gilbert, M. White: Application of the parabolic equation to sound propagation in a refracting atmosphere. *J. Acoust. Soc. Am.* **85** (1989) 630–63.
- [6] D. Lee, A. Pierce: Parabolic equation development in recent decade. *J. Comp. Acoust.* **3**(2) (1995) 95–173.
- [7] C. Bailly, P. Blanc-Benon: Stochastic turbulent fields for acoustic numerical simulation. Proceedings of the ASME, NCA-Vol.2, 1998. 21–33.
- [8] P. Chevret, P. Blanc-Benon, D. Juvé: A numerical model for sound propagation through a turbulent atmosphere near the ground. *J. Acoust. Soc. Am.* **100** (1996) 3587–3599.
- [9] Y. Hugon-Jeannin: Simulation numérique de la propagation d'ondes acoustiques en milieu turbulent. Dissertation. Ecole Centrale de Lyon, ECL, n° 92-3, 1992.
- [10] M. Karweit, P. Blanc-Benon, D. Juvé, G. Comte-Bellot: Simulation of the propagation of an acoustic wave through a turbulent velocity field: A study of phase variance. *J. Acoust. Soc. Am.* **89**(1) (1991) 52–62.
- [11] D. Wilson, D. Thomson: Acoustic tomographic monitoring of the atmospheric boundary layer. Tech. Rept. TR 92–002, Applied Research Lab, The Pennsylvania State University, State College, USA, 1992.
- [12] K. Wert, P. Blanc-Benon, D. Juvé: Effect of turbulence scale resolution on numerical simulation of atmospheric sound propagation. In 4th AIAA/CEAS Aeroacoustics Conference, Toulouse, France, 1998. AIAA n° 98–2245, 246–256.
- [13] D. Juvé, P. Blanc-Benon, K. Wert: Numerical simulation of sound propagation through time-dependent random media. – In: Theoretical and Computational Acoustics'97. Y.-C. Temg, E.-C. Shang, Y.-H. Pao, H. Schultz, A. Pierce (eds.). World Scientific Publishing Co, New-York, 1997, 653–665.
- [14] G. Comte-Bellot, S. Corrsin: Simple eulerian time correlation of full-narrow-band velocity signals in grid generated 'isotropic' turbulence. *J. Fluid Mech.* **48** (1971) 273–337.
- [15] P. Blanc-Benon, D. Juvé, M. Karweit, G. Comte-Bellot: Simulation numérique de la propagation des ondes acoustiques à travers une turbulence cinématique. *J. Acoust* **3**(1) (1990) 1–8.
- [16] J. Wasier: Etude expérimentale des effets d'une frontière sur la propagation des ondes acoustiques à travers une turbulence thermique. Dissertation. Ecole Centrale de Lyon, ECL, n° 1999-46, 1999.
- [17] K. M. Li, Q. Wang: Analytical solution for outdoor sound propagation in the presence of wind. *J. Acoust. Soc. Am.* **102** (1997) 2040–2049.
- [18] K. Gilbert, R. Raspet, X. Di: Calculation of turbulence effects in an upward-refracting atmosphere. *J. Acoust. Soc. Am.* **87** (1990) 2428–2437.
- [19] D. Thomson, D. Wilson, D. Havelock: The effect of turbulent intermittency on scattering into a shadow zone. *J. Acoust. Soc. Am.* **99** (1996) 3393–3400.
- [20] B. Kader, A. Yaglom: Spectra and correlation functions of surface layer atmospheric turbulence in unstable thermal stratification. – In: Selected papers from "Turbulences 89 : organized structures and turbulence in fluid mechanic. M. Lesieur, O. Métais (eds.). Kluwer Academic Publisher, Amsterdam, 1991, 387–411.
- [21] S. Khanna, J. Brasseur: Analysis of monin-obukhov similarity from large-eddy simulation. *J. Fluid Mech.* **345** (1997) 251–286.
- [22] D. Wilson: On the application of turbulence spectral / correlation models to sound propagation in the atmosphere. Proc. Eighth International Symposium on Long Range Sound Propagation, Applied Research Lab., The Pennsylvania State University, 1998. 296–312.
- [23] P. Blanc-Benon, D. Juvé, G. Comte-Bellot: Occurrence of caustics for high-frequency acoustic waves propagating through turbulent field. *Theor. and Comp. Fluid Dyn.* **2** (1991) 271–278.
- [24] D. Juvé, P. Blanc-Benon, P. Chevret: Sound propagation through a turbulent atmosphere: influence of the turbulence model. Proc. Sixth International Symposium on Long Range Sound Propagation, NRC, Ottawa, Canada, 1994. 270–282.
- [25] L. Dallois, P. Blanc-Benon, D. Juvé: A wide angle parabolic equation for sound waves in inhomogeneous moving media: Applications to atmospheric sound propagation moving media. *J. Comp. Acous.* **9**(2) (2001) 477–494.